



OPEN Chlorogenic acid promotes fatty acid beta-oxidation to increase hESCs proliferation and lipid synthesis

Ming Zong^{1,2,6}, Jingzhang Ji^{2,6}, Qinglai Wang^{3,6}, Yizhen Cai⁴, Lijun Chen², Lixin Zhang², Weibo Hou², Xuanwen Li², Qingran Kong², Cunqing Zheng⁵, Jiaming Zhang²✉, Qi Zhao²✉ & Wenpin Cai¹✉

Cell metabolism plays a crucial role in regulating the pluripotency of human embryonic stem cells (hESCs). Chlorogenic acid (CGA), an essential dietary polyphenol, exhibits diverse pharmacological effects on metabolism regulation. This study examines the effects of CGA on cell metabolism in hESCs using the H9 model. At a concentration of 100 µg/ml, CGA showed low toxicity and had no impact on the viability of H9 cells. Furthermore, it promotes *NANOG* expression. Importantly, CGA enhances Fatty acid β-oxidation (FAO), thus promoting the proliferation and lipid synthesis of H9 cells. Mechanistically, CGA-induced FAO generates acetyl-CoA, which enhances *de novo* lipid synthesis and hyperacetylates H3K27 at the promoter regions of associated genes, thereby enhancing their expression. This study highlights the potential beneficial effects of CGA on cell proliferation and provides opportunities for optimizing the in vitro culture of hESCs.

Pluripotent embryonic stem cells have the ability to self-renew indefinitely and differentiate into all types of adult cells, thus holding promising prospects in regenerative medicine applications such as tissue replacement therapy^{1–3}. Human embryonic stem cells (hESCs) are derived from the inner cell mass of blastocyst and can maintain their pluripotent state in vitro under certain cultural conditions for extended periods⁴. The transcription factors *Nanog*, *Pou5f1*, and *Sox2* have long been central to the pluripotency network of hESCs; their interaction with each other, as well as many other pluripotency factors, play a crucial role in maintaining the pluripotency^{5,6}. At the same time, the expressions of these key transcription factors endow hESCs with unique cell cycle and proliferation characteristics. Previous study has shown that *Nanog* can regulate the cell cycle independently via the ERas/phosphatidylinositol 3-kinase/Akt pathway without affecting pluripotency⁷. Therefore, the understanding of the key molecular mechanisms involved in regulating the self-renewal network are required.

Cell metabolism plays a critical role in regulating the self-renewal, quiescence, and differentiation potential of stem cells⁸. Previous studies have shown that embryonic stem cells (ESCs) possess a unique metabolic pattern distinct from differentiated cells^{9,10}. Metabolic pathways regulate stem cell manners by generating energy and metabolites¹¹. For example, ESCs enhance glycolysis and glutamine oxidation to provide intermediates, promoting macromolecular biosynthesis to support the self-renewal¹². Therefore, a more comprehensive understanding of stem cell metabolism can allow us to improve cultural conditions, thereby increasing stem cell expansion and functionality.

Lipid metabolism is needed by cells for membrane biogenesis, energy production and protein modification¹³. Fatty acid β-oxidation (FAO) results in the shortening of fatty acids by two carbons per cycle, generating acetyl-CoA, which is a very efficient source for *de novo* synthesis of lipids¹⁴. FAO is not only a key pathway for energy

¹Department of Laboratory Medicine, Wenzhou TCM Hospital of Zhejiang Chinese Medical University, Wenzhou 325000, Zhejiang, China. ²Oujiang Laboratory, Zhejiang Provincial Key Laboratory of Medical Genetics, Key Laboratory of Laboratory Medicine, School of Laboratory Medicine and Life Sciences, Ministry of Education, Wenzhou Medical University, Wenzhou 325035, Zhejiang, China. ³The department of Orthopedics and traumatology Medicine, Wenzhou TCM Hospital of Zhejiang Chinese Medical University, Wenzhou 325000, Zhejiang, China. ⁴The Second School of Medicine, Wenzhou Medical University, The Second Affiliated Hospital and Yuying Children's Hospital of Wenzhou Medical University, Wenzhou 325000, Zhejiang, China. ⁵Department of Clinical Laboratory, Wenzhou Seventh People's Hospital, Wenzhou 325000, Zhejiang, China. ⁶Ming Zong, Jingzhang Ji and Qinglai Wang have contributed equally to this work. ✉email: jmzhang1225@163.com; zq920@163.com; cwp1820@163.com

generation but is also closely linked to multiple metabolic regulatory mechanisms. Studies have shown that FAO enhances ATP production by providing acetyl-CoA to mitochondria, supporting cellular metabolic activities under high energy demand conditions. For pluripotent stem cells, especially hESCs, FAO serves not only as a tool for energy provision but is also closely associated with signaling pathways that regulate cell growth, metabolic balance, and metabolism-related epigenetic modifications. Specifically, the acetyl-CoA produced by FAO can not only enter the tricarboxylic acid cycle to provide energy but also participate in histone acetylation reactions, regulating chromatin openness and thereby influencing the transcriptional activity of pluripotency-related genes. For example, FAO may promote the formation of histone modifications such as H3K27ac by increasing the supply of acetyl-CoA, which has been shown to be closely related to the expression of pluripotency-maintaining factors like Nanog, Oct4, and Sox2. Moreover, increased FAO activity has been observed in proliferating naïve-state hESCs, but the molecular mechanisms of FAO's role in hESCs proliferation remain to be elucidated.

Chlorogenic acid (CGA), a vital bioactive dietary polyphenol, is abundantly present in various plants such as *Eucommia*, honeysuckle, coffee, potatoes, apples, and tea¹⁵. It exhibits a wide range of pharmacological effects, including antioxidant, antibacterial, antiviral, anticancer, lipid-lowering, blood sugar reduction, and immunomodulatory actions^{16–22}. Previous studies have explored the crucial role of CGA in FAO^{23–25}. However, the specific roles and mechanisms by which CGA regulates fatty acid metabolism in hESCs remain unclear, despite previous investigations into the important role of *de novo* lipid synthesis as a common transcriptional characteristic of human pluripotent stem cells (hPSCs) cultured in E8 and pre-implantation human epiblast *in vivo*²⁶. In this study, we observed that CGA enhances the proliferation capacity and *de novo* lipid synthesis of H9 by promoting FAO and Nanog expression levels.

In addition, we further explored the critical role of CGA-activated key metabolic pathways in hESCs in regulating pluripotency of hESCs. Previous studies have shown that CGA plays a significant role in maintaining normal metabolism by impacting carbohydrate metabolism, lipid synthesis and breakdown, as well as amino acid metabolism^{27,28}. In hESCs, glycolysis is considered a key pathway for maintaining pluripotency and proliferation, while mitochondrial function further supports the cell's metabolic needs through the synergistic action of FAO and glycolysis. Specifically, CGA may regulate energy balance in hESCs by promoting the interaction between FAO and the glycolytic pathway, thereby supporting self-renewal and maintaining pluripotency. CGA may provide the necessary metabolic support for hESCs by facilitating the interaction between these pathways, enhancing their proliferative capacity.

Results

CGA elevates NANOG expression and proliferation of H9

To examine the effect of CGA on hESCs, we introduced CGA into E8 medium and cultured H9 hESCs for either 24–48 h at varying concentrations. Our findings indicate that CGA at a concentration of 100 µg/ml had no significant impact on cell viability, as determined by the CCK8 assay (Fig. 1A). However, at a concentration of 1000 µg/ml, CGA significantly decreased H9 cell viability (Fig. 1B), demonstrating a low level of toxicity. Based on these results, we selected the addition of 100 µg/ml CGA for a duration of 24 h for subsequent analysis.

Interestingly, the addition of CGA resulted in an increase in the colony size of H9 hESCs (Fig. 1C), suggesting a positive effect on their proliferation. We subsequently investigated the impact of CGA on the pluripotency of hESCs by examining the expression of pluripotency markers *POU5F1*, *SOX2*, and *NANOG* in H9 cells. We observed a significant upregulation of *NANOG*, but no change in *POU5F1* and *SOX2* expression (Fig. 1D–F). This elevation in *NANOG* expression was further confirmed through immunofluorescence analysis (Fig. 1G). Our results indicate that CGA has the potential to enhance *NANOG* expression and promote the proliferation of hESCs.

CGA enhances lipid synthesis and proliferation of H9 by activation of FAO

To investigate the mechanism underlying the effects of CGA on pluripotency in hESCs, we conducted RNA sequencing (RNA-seq) of CGA-treated H9 cells. Differential gene analysis revealed significant changes in the transcriptome, with 1,044 genes upregulated and 273 genes downregulated (Fig. 2A; Supplementary Table S1; Fold change > 1.4, Fold change < -1.4, $p < 0.05$). Gene Ontology (GO) analysis demonstrated that upregulated genes were enriched in pathways related to the inactivation of MAPK, cell cycle regulation, and fatty acid metabolism (Fig. 2B). Conversely, downregulated genes were enriched in pathways related to MAPK and transcription regulation (Fig. 2C). Notably, gene set enrichment analysis (GSEA) indicated that many of the genes upregulated by CGA treatment were associated with fatty acid metabolism (Fig. 2D). These findings suggest that CGA may enhance FAO in hESCs.

To investigate the effect of CGA on the pluripotency of hESCs through the hyperactivation of FAO, we utilized trimetazidine (TMZ) as an inhibitor of the HADHA/B enzyme in the FAO pathway in the CGA-treated H9 cells (referred to as the CGA + TMZ-treated group; Fig. 2E). Subsequently, transcriptome sequencing data was generated for the CGA + TMZ-treated group. Unsupervised hierarchical clustering (MHC) analysis demonstrated a strong correlation between the CGA + TMZ-treated group and the vehicle group at the transcriptional level (Fig. 2F). Comparative gene expression analysis revealed the restoration of expression in CGA + TMZ-treated H9 cells for key genes involved in the FAO pathway, including *CPT1C*, *CPT2*, *ACAA2*, *HADHA*, and *HADHB* (Fig. 2G). Further analysis of RNA-seq data identified 72 genes associated with fatty acid synthesis and 27 genes linked to the G1/S transition of the mitotic cell cycle. Notably, these genes were found to be upregulated in the CGA-treated group and downregulated in the CGA + TMZ-treated group (Fig. 2H). This suggests that CGA-induced lipid synthesis and proliferation in hESCs may be attributed to the activation of FAO.

To validate the phenomenon, we initially utilized Compass to investigate the activity of fatty acid metabolism at the metabolic level. The metabolites related to fatty acid synthesis, such as palmitoleic acid, oleic acid, and stearic acid, were projected to increase in the CGA-treated group and decrease in the CGA + TMZ group (Fig. 2I).

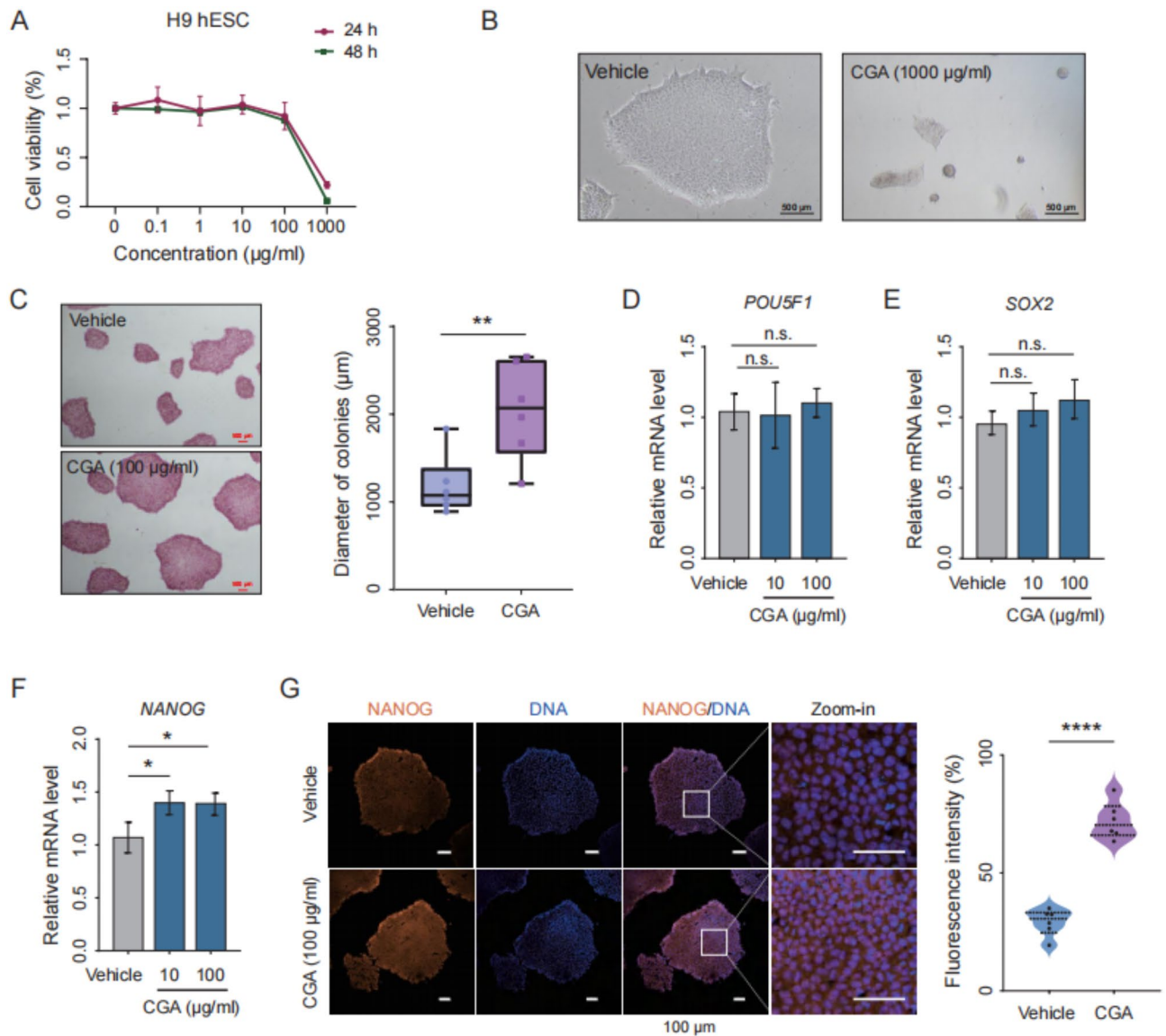
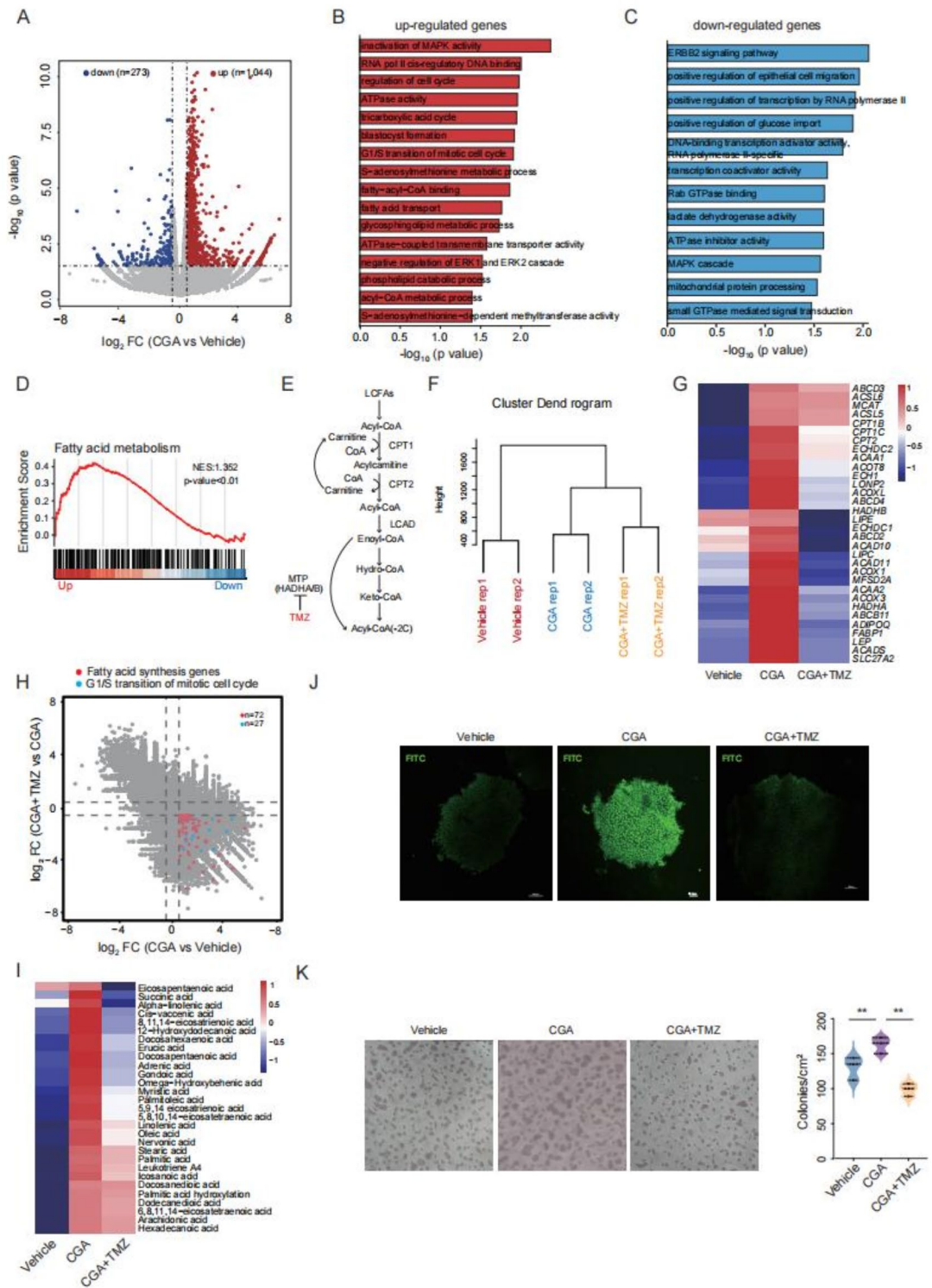


Fig. 1. Effect of CGA on the pluripotency of H9. (A) CCK-8 assays were conducted to test the cell viability of H9 cells treated with different concentrations of CGA for 24 h and 48 h. Each group had five replicates. (B) Representative images of H9 clones in the vehicle group and the group treated with 1000 µg/ml CGA for 24 h. Vehicle group added an equal amount of 50% ethanol as the solvent control in H9 cell line. (C) Alkaline phosphatase staining was performed, and the diameters of H9 clones in the vehicle group and the group treated with 100 µg/ml CGA were measured. Statistically significant differences were observed (** $p < 0.01$, Student's t-test). (D–F) RT-qPCR was used to analyze the expression of *POU5F1* (D), *SOX2* (E), and *NANOG* (F) in the vehicle group and the group treated with 100 µg/ml CGA. The data represent means \pm SEM from three independent experiments. No statistically significant differences were observed when compared to the vehicle group (n.s. > 0.05), except for *NANOG* expression where a significant difference was observed (* $p < 0.05$). (G) Representative confocal images of H9 cells stained with NANOG antibody in the vehicle group and the group treated with 100 µg/ml CGA. The scale bar represents 100 µm. Quantification of NANOG fluorescence intensity showed a highly significant difference between the two groups (**** $p < 0.0001$, Student's t-test).

This was further confirmed by BODIPY 493/503 staining (Fig. 2J). Additionally, treatment of H9 cells with CGA + TMZ restored the size of colonies (Fig. 2K), indicating that the heightened FAO activation contributes to CGA-induced cell proliferation. In summary, these findings suggest that CGA has the ability to promote lipid synthesis and proliferation of hESCs through the activation of FAO.

CGA maintains H9 pluripotency

We conducted further investigation to determine if the impact of CGA on the pluripotency regulatory network is influenced. This was accomplished by analyzing the transcriptomics of vehicle, CGA, and CGA + TMZ-



treated H9 cells. Our findings indicated that there were no significant changes in the transcription patterns of pluripotency genes, such as *POU5F1*, *POU3F1*, *SOX2*, *SALL2*, and *SOX15*, following treatment with CGA and TMZ. However, we did observe a significant upregulation in the expression of *NANOG* by CGA, which was not significantly downregulated in the CGA + TMZ-treated group. This suggests that the regulation of *NANOG* expression by CGA may not occur through FAO. Interestingly, we also observed that the expression of *OTX2*, which plays a role in cell proliferation during mitosis, was significantly upregulated by CGA and downregulated in the CGA + TMZ-treated group. This could potentially contribute to enhanced proliferation of hESCs (Fig. 3A). Furthermore, we utilized ScoreCard analysis to quantify the differentiation potential of hESCs, and interestingly, found no preferential differentiation in the CGA- and CGA + TMZ-treated H9 cells (Fig. 3B). These findings suggest that CGA does not have an effect on the pluripotency of hESCs.

Fig. 2. CGA regulates fatty acid synthesis and proliferation of H9 by FAO. **(A)** Volcano plot displaying the impact of CGA on the transcriptome of H9. ($FC > 1.4$, $FC < -1.4$, $p < 0.05$.) **(B–C)** GO analysis of differentially expressed genes in CGA-treated H9: red indicates pathways enriched in up-regulated genes **(B)**, while blue indicates pathways enriched in down-regulated genes **(C)**. **(D)** GSEA of fatty acid metabolism-associated genes showing preferential upregulation in CGA-treated H9. **(E)** Scheme of long chain fatty acids (LCFAs) into fatty acid oxidative (FAO) metabolism, showing the targets of TMZ. **(F)** Unsupervised clustering of transcriptomes in vehicle, CGA, and CGA + TMZ-treated groups. **(G)** Heatmap of fatty acid β -oxidation genes in H9 in the indicated groups. **(H)** Scatterplots of RNA-seq data of H9 in CGA-treated versus vehicle groups (x-axis) and CGA + TMZ versus CGA-treated groups (y-axis). Red dots and blue dots represent genes related to fatty acid synthesis and G1/S transition of mitotic cell cycle, respectively. **(I)** Prediction of long-chain fatty acid metabolites by COMPASS. **(J)** BODIPY 493/503 staining revealed increased fatty acids in CGA-treated H9 but rescued by TMZ. **(K)** Diameters of H9 clones in the indicated treatments. (** $p < 0.01$, Student's t-test).

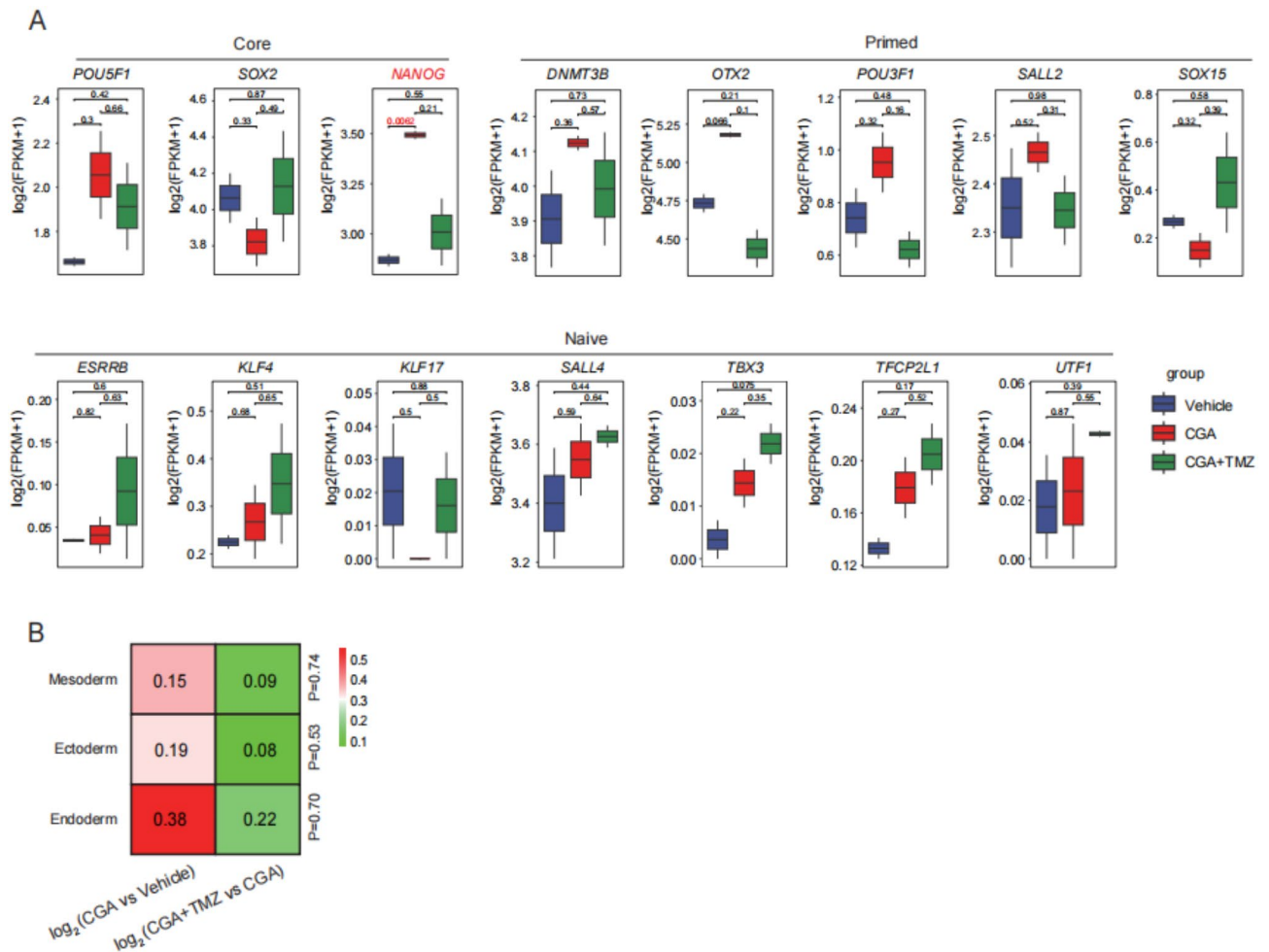


Fig. 3. CGA regulates the regulatory network of pluripotency in H9 through FAO. **(A)** Transcriptome analysis was conducted to determine the expression levels of pluripotency markers in hESCs under different treatment conditions: vehicle, CGA, and CGA + TMZ-treated H9 cells. **(B)** ScoreCard analysis was performed to assess the lineage tendencies of hESCs under the indicated treatments.

CGA regulates H9 metabolic state

Previous studies have demonstrated the potential role of CGA in regulating cell metabolism^{29–31}. To investigate the impact of CGA on metabolic reprogramming in hESCs, we initially assessed the expressions of genes associated with four key metabolic pathways: glycolysis, the TCA cycle, OXPHOS, and one-carbon metabolism. The expression levels of genes related to these pathways, such as *GCK*, *PGK1*, *ENO2* for glycolysis; *SDHC*, *ADH1*, *IDH2* for the TCA cycle; *NDUFS1*, *COX4I2*, *COX7A1* for OXPHOS; and *FPGS*, *MAT2A*, *MTHFD1* for one-carbon metabolism, were significantly increased in the CGA-treated group. Importantly, the expression levels of most genes were rescued after CGA + TMZ treatment. (Fig. 4A). Furthermore, the changes in metabolites, such as pyruvate, glucose 1-phosphate, fructose 6-phosphate for glycolysis; oxaloacetate, malate, citrate for the

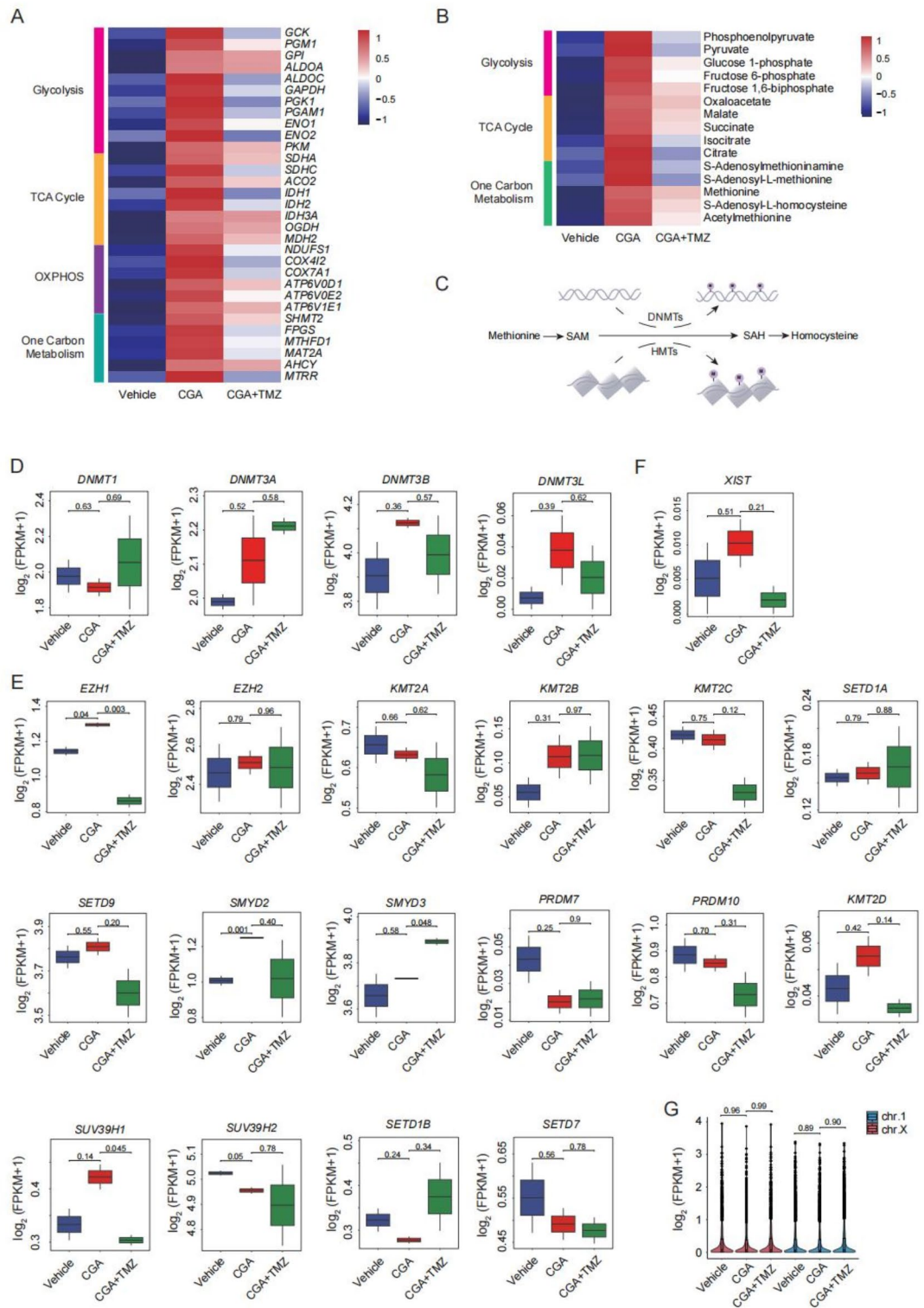


Fig. 4. Metabolic reprogramming by CGA treatment in H9 cells. **(A)** The heatmap illustrates gene expressions associated with metabolic pathways in the vehicle, CGA, and CGA + TMZ-treated H9 cells. **(B)** The heatmap visualizes changes in intermediate metabolites linked to metabolic pathways in the vehicle, CGA, and CGA + TMZ-treated H9 cells. **(C)** This schematic diagram depicts the one-carbon metabolism pathway, which provides methyl donors for DNA and histone methylation. **(D–F)** Transcriptome analysis reveals the expression levels of DNA methyltransferase genes **(D)**, histone methyltransferase genes **(E)**, and *XIST* **(F)** in the vehicle, CGA, and CGA + TMZ-treated H9 cells. **(G)** The violin plot demonstrates the expression levels of genes located on Chromosome X and Chromosome 1 in the vehicle, CGA, and CGA + TMZ-treated H9 cells.

TCA cycle; and S-adenosyl-L-methionine (SAM), methionine, S-Adenosyl-L-homocysteine for one-carbon metabolism, were predicted by Compass (Fig. 4B).

Among them, SAM from one-carbon metabolism was found to be the most dynamic. SAM plays a crucial role in chromatin reprogramming by providing one-carbon units for DNA and histone methylation^{32,33} (Fig. 4C). However, there were no significant changes observed in the transcription of DNA methyltransferases, such as *DNMT1*, *DNMT3A*, and *DNMT3B* (Fig. 4D). This suggests that the DNA methylation state of hESCs is not influenced by CGA. In terms of histone methylation, only *EZH1*, a component of a noncanonical polycomb repressive complex-2 (PRC2), was significantly upregulated and downregulated in the CGA and CGA + TMZ-treated H9, respectively (Fig. 4E). This may provide further specificity to PRC2 action following CGA treatment. To determine the effects of CGA on X-chromosome inactivation, we analyzed the X-chromosome states in vehicle, CGA, and CGA + TMZ-treated H9 using RNA-seq analysis. Interestingly, we observed no significant alterations in the expressions of *XIST* and X chromosome genes³⁴ (Fig. 4F, G). This indicates that CGA has no effect on the activity of the X-chromosome. Taken together, these results suggest that CGA may regulate the metabolic state of hESCs without significantly affecting DNA and histone methylations.

CGA induces H3K27 hyperacetylation to promote lipid synthesis in H9

The results above demonstrate that CGA promotes FAO in H9 (Fig. 2G-I). FAO produces acetyl-CoA, which is not only an efficient source for lipid synthesis, but also serves as a substrate for enzymes involved in histone acetylation^{35–37}. Based on this, we hypothesized that CGA treatment may lead to changes in histone acetylation (Fig. 5A). To test this hypothesis, we analyzed various acetylation marks on histone H3 (H3K18ac, H3K27ac, and H3K9ac) using publicly available data. Each of these marks has been shown to play a significant role in defining chromatin states and regulating gene expression. Among them, H3K27ac has the highest genome coverage (Fig. 5B), suggesting that it may be particularly important in maintaining the pluripotent state of hESCs.

Immunofluorescence staining was conducted to assess H3K27ac expression, revealing a significant increase in H3K27ac levels with CGA treatment and a decrease with CGA + TMZ treatment (Fig. 5C). To further investigate the impact of H3K27ac in CGA-treated H9, the H3K27ac landscape was profiled using cleavage under targets and tagmentation (CUT&Tag) in the vehicle, CGA, and CGA + TMZ-treated cells. The three groups were clearly distinguished by MHC (Fig. 5D). Notably, CGA treatment led to a marked enhancement of H3K27ac signals, specifically at gene promoter regions, which were subsequently reversed upon TMZ supplementation (Fig. 5E, F). These findings suggest that CGA may modulate gene expression by influencing H3K27ac patterns.

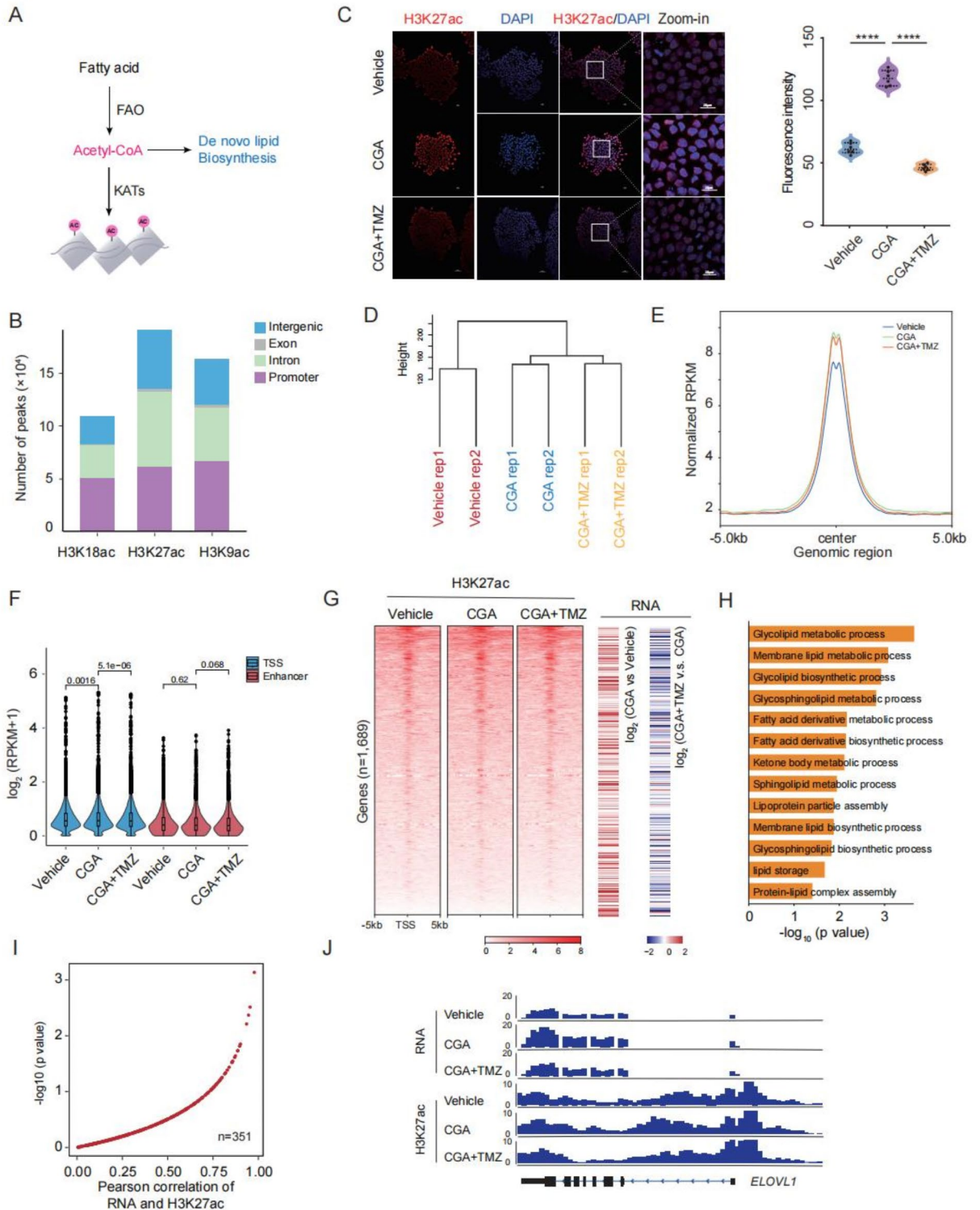
To further elucidate the changes in gene expression mediated by CGA and H3K27ac, we conducted a joint analysis of RNA-seq and H3K27ac CUT&Tag data. Our findings reveal that the hyperacetylation of H3K27 in the promoter regions of certain genes ($n = 1,689$), induced by CGA, was partially restored by TMZ supplementation, consequently leading to a decrease in their expressions (Fig. 5G). Importantly, GO analysis demonstrated that the majority of these genes were closely associated with fatty acid metabolisms (Fig. 5H). Moreover, the expressions of 351 genes involved in fatty acid metabolism positively correlated with the enrichment of H3K27ac in the promoter regions (Fig. 5I), such as *ELOVL1* (Fig. 5J), which is responsible for elongating long chain fatty acids³⁸. Overall, these results suggest that the acetyl-CoA generated through CGA-mediated fatty acid oxidation not only serves as a substrate for lipid synthesis but also induces hyperacetylation of H3K27 to enhance the expressions of genes related to fatty acid metabolism in human embryonic stem cells.

Discussion

In this study, we investigated the impact of CGA on the metabolism of fatty acids in hESCs. With the use of the H9 model, we discovered that CGA actively stimulated cell proliferation by activating FAO. Furthermore, CGA also boosted the production of acetyl-CoA through enhanced FAO, which in turn promoted the synthesis of new lipids and the upregulation of genes associated with lipid metabolism. These effects were observed through the process of H3K27 hyperacetylation. Our findings suggest that CGA holds potential in providing beneficial effects for hESCs (Fig. 6).

ESCs have a high demand for synthetic metabolic precursors, which are crucial for replicating their genome, cytoplasm, and organelles. In this study, we have shown the regulatory role of CGA in promoting FAO in (h)ESCs. Previous research has demonstrated that FAO is essential for the self-renewal of adult stem cells and is also involved in sustaining the self-renewal of breast cancer stem cells and supporting tumor survival under metabolic stress conditions³⁹. Similarly, our findings indicate that CGA-induced FAO promotes the proliferation of hESCs. Ground state ESCs heavily rely on elevated FAO for oxidative phosphorylation and energy production. When FAO/oxidative phosphorylation is inhibited, naïve hESCs enter a state of pluripotent quiescence, characterized by small, dome-shaped colonies and sustained expression of pluripotency markers⁴⁰. We observed that CGA-activated FAO increased the expression of *Nanog*, but not *Pou5F1* and *Sox2*, highlighting the role of *Nanog* in regulating hESCs proliferation. The increase in *Nanog* expression after FAO activation may indicate an enhanced self-renewal ability of hESCs through the FAO signaling pathway. Specifically, fatty acid oxidation might indirectly influence the metabolic environment required for stem cell self-renewal by improving mitochondrial function and energy metabolism. Further experiments can investigate whether FAO activation regulates the expression of self-renewal-related genes by upregulating *Nanog*. Additionally, there is a complex balance between *Nanog* expression levels and differentiation potential. For instance, moderate *Nanog* expression may promote certain types of differentiation, while *Nanog* overexpression might maintain an undifferentiated state and inhibit differentiation. Thus, *Nanog* upregulation caused by FAO activation may have a bidirectional effect on hESCs differentiation potential, depending on the intensity of FAO activation and its specific regulation of cellular metabolism.

The active FAO can also promote *de novo* lipid synthesis by supplying acetyl-CoA. Lipids are vital for maintaining cellular homeostasis, as they provide macromolecules for membrane biosynthesis during growth



and proliferation⁴¹. Cell proliferation is closely linked to the *de novo* synthesis of lipids. Therefore, we attribute the enhanced proliferation of hESCs to the lipid synthesis induced by CGA-mediated FAO. FAO can oxidize medium and long-chain fatty acids in order to produce acetyl-CoA⁴². Acetyl-CoA is a key precursor in lipid synthesis and also serves as an acetyl donor for histone acetylation^{36,43}. In this study, we observed that CGA promotes H3K27ac through FAO. The promoter regions of lipid synthesis-associated genes showed hyperacetylation of H3K27, thereby enhancing their expression. Thus, a positive feedback loop occurs for FAO-mediated lipid synthesis induced by CGA in hESCs.

In summary, our study revealed that CGA enhances the proliferation and lipid synthesis of hESCs by promoting FAO. Mechanistically, CGA-induced FAO generates acetyl-CoA, which in turn facilitates *de novo* lipid synthesis. Additionally, CGA hyperacetylates H3K27 at the promoter regions of genes associated with lipid

Fig. 5. CGA induces H3K27 hyperacetylation in H9. **(A)** Scheme illustrating the FAO production of acetyl CoA for *de novo* lipid synthesis and histone acetylation. **(B)** Distribution of H3K9ac, H3K18ac, and H3K27ac peaks in promoter, intron, exon, and intergenic regions of H9, expressed as percentages. **(C)** Representative confocal images of H9 cells treated with Vehicle, CGA, and CGA + TMZ, stained with H3K27ac antibody. Scale bar represents 20 μm . Quantification of H3K27ac fluorescence intensity (**** $p < 0.0001$, Student's t-test). **(D)** MHC analysis of H3K27ac signals in H9 cells under the indicated treatments. **(E)** Normalized signal intensity of H3K27ac across the genome in H9 cells under the indicated treatments. **(F)** Violin plot showing significant upregulation of H3K27ac signals at transcriptional start sites (TSS) in the CGA-treated group compared to the vehicle and CGA + TMZ-treated groups. **(G)** Heatmap (left) displaying relative changes in H3K27ac signals among H9 cells under the indicated treatments. Heatmap (right) shows expression changes of genes between the indicated groups. **(H)** GO analysis of the genes in panel (G). **(I)** Pearson correlation analysis of RNA and H3K27ac enrichment at the promoters of genes involved in lipid biosynthesis. **(J)** Genome browser view of H3K27ac signals at the *ELOVL1* locus in H9 cells under the indicated treatments.

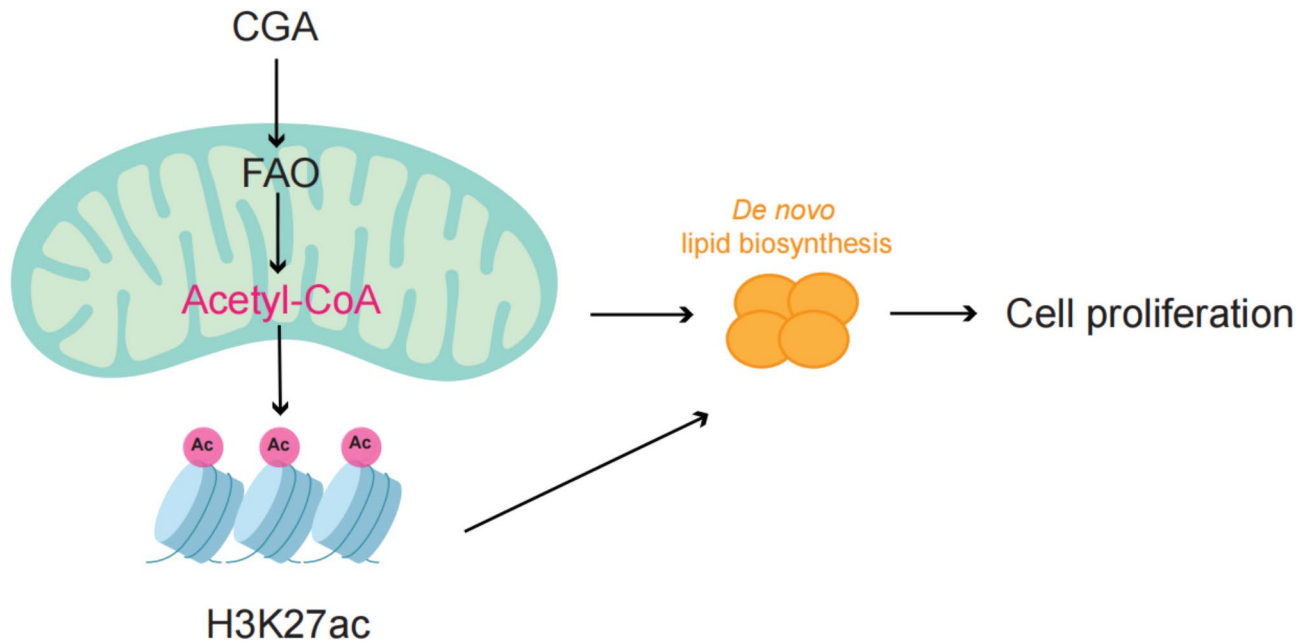


Fig. 6. Schematic diagram of CGA promotes FAO to increase hESCs proliferation and lipid synthesis.

synthesis, leading to enhanced gene expression. These findings demonstrate the potential beneficial effects of CGA on hESCs. Furthermore, our study provides an avenue for optimizing the *in vitro* culture of hESCs.

CGA-induced FAO promotes cell proliferation and *de novo* lipid synthesis in H9 cells. Additionally, CGA enhances FAO, leading to the production of acetyl-CoA, which further promotes *de novo* lipid synthesis and increases the expression of genes associated with lipid synthesis through H3K27 hyperacetylation.

Materials and methods

Cell culture

The H9 cell line of hESCs was generously provided by Professor Ling Shuai from Nankai University. In accordance with the WiCell Feeder Independent Pluripotent Stem Cell Protocols from the University of Wisconsin, the hESCs are cultured on Matrigel-coated dishes using E8 medium. To initiate the culture, a mixture of 200 μl Matrigel and 12 ml DMEM/F-12 medium is prepared and 1 ml of this solution is added per well in a 6-well plate. The plate is then incubated at 37 $^{\circ}\text{C}$ in a cell culture incubator for 90 min, after which any excess Matrigel is removed prior to cell inoculation. The E8 hESCs are passed every 3–4 days using an EDTA dissociation buffer containing 0.5 mM EDTA in DPBS. The cells are first washed twice with DPBS, followed by incubation with the EDTA dissociation buffer at 37 $^{\circ}\text{C}$ for 5 min. After removing the EDTA, 1 ml of E8 medium is added to the culture dish. Gently agitating the dish facilitates the formation of high-quality small clones, which are subsequently passaged at a ratio of 1:10 to 1:20.

Cell viability assays

The cells were seeded in 96-well plates with five duplicate wells in each group. Around the sample wells, 100 μl of DPBS was added to prevent liquid evaporation. After the cells adhered to the wall, different concentrations of drug-treated medium were replaced, and the blank vehicle groups were set. The IC₅₀ assay was performed using the CCK8 kit (Dojindo, Kyushu, Japan), and cell proliferation was determined at specified times following

the manufacturer's protocol. Cell viability was measured by determining the absorbance at 450 nm. The formula used for calculation was as follows: cell viability (%) = $[A(\text{treat}) - A(\text{blank})] / [A(\text{vehicle}) - A(\text{blank})] \times 100$.

Alkaline phosphatase staining

Alkaline phosphatase staining was performed using the Alkaline Phosphatase Staining Kit II (00-0055, Stemgent, Hamburg, Germany) according to the manufacturer's instructions. The residual culture medium was washed away with 1×PBS, and this step was repeated twice. Subsequently, the cells were fixed with 4% PFA for 10 min. A 1×PBST solution was prepared by adding 5 µl of Tween 20 to 10 ml of 1×PBS, resulting in a final concentration of 0.05%. The fixation solution was discarded, and the residual polyformaldehyde was washed away with 1×PBST, repeating this step twice. To prepare the AP substrate solution, 500 µl of Solution A was mixed with 500 µl of Solution B for each well, and the mixture was left to stand at room temperature for 2 min. Then, the required volume of Solution C (500 µl) was added to each well, and the working solution was mixed. The 1×PBST was discarded, and 1.5 ml of the working solution was added. The cells were incubated in darkness at room temperature for 10 min. Afterward, the excess staining solution was washed off with 1×PBST, and the cells were air-dried. Finally, the cell colonies were counted to evaluate the proliferation ability of hESCs.

BODIPY

Prepare cell slides in advance in a 24-well cell culture plate, add 500 µl of Matrigel to the 24-well plate with prepared slides to ensure close contact between the slides and the bottom of the culture dish, and incubate at 37 °C for 90 min. After preparation, inoculate cells of suitable density according to routine procedures for wall attachment growth. Stain when cell confluence reaches 70%. Wash 3 times with DPBS, then fix for 15 min with 4% paraformaldehyde (PFA). Remove the fixative and wash 3 times with DPBS. Incubate the fixed cells with 1 µg/ml BODIPY 493/503 (molecular probe) in DPBS for 30 min, and observe imaging under a confocal laser microscope.

RT-qPCR

Total RNA was extracted using the Arcturus PicoPure RNA Isolation Kit (12204-01; Ambion, Austin, TX, USA) according to the manufacturer's instructions, and reverse transcription was performed to generate cDNA using the PrimeScript RT Master Mix (RR036; Takara, Kusatsu, Japan). The RNase-Free DNase Set (79254; Qiagen, Hilden, Germany) was used to ensure that there was no DNA contamination. We performed RT-qPCR using the TB Green Premix Ex Taq II (RR820; Takara) and CFX96 Real-Time System (Bio-Rad, Hercules, CA, USA). The reaction parameters were as follows: 95 °C for 30 s, followed by 40 two-step cycles of 95 °C for 5 s and 60 °C for 34 s. *GAPDH* was used as a reference gene. Ct values were calculated using the BioRadCFXManager software (version 2.2 <https://en.freownloadmanager.org/Windows-PC/Bio-Rad-CFX-Manager.html>), and the target sequences were normalized to the reference sequence using the $2^{-\Delta\Delta C_t}$ method.

Immunofluorescence staining

After removing the zona pellucida with acidic operating fluid, cells were fixed for 15 min at room temperature in 4% PFA, followed by permeabilization in 10% Triton X-100 for 40 min at 37°C. Cells were then blocked-in blocking solution consisting of 1% bovine serum albumin (BSA) in phosphate-buffered saline (PBS) for 1 h at 37°C after three washes in washing solution (0.1% Tween-20, 0.01% Triton X-100 in PBS). Incubations were performed overnight at 4 °C using the following antibodies and dilutions in blocking solution: anti-NANOG (1:100; ab21624; Abcam, Cambridge, UK), anti-H3K27ac (1:100; ab4729; Abcam). Then, the cells were washed three times in washing solution and incubated with secondary antibodies: Alexa Fluor 546-conjugated donkey anti-rabbit IgG (1:500; A10040; Invitrogen, Carlsbad, CA, USA) for 1 h at 37°C. Samples were mounted onto slides with antifade medium containing DAPI (C1005; Beyotime, Shanghai, China) and examined under TCS SP8 inverted confocal microscope.

RNA-seq library preparation

RNA-seq libraries were prepared as previously described⁴⁴. Briefly, every 50 cells from a dish were pooled for one group. All groups were amplified to obtain cDNA by the SMART-Seq2 protocol (N712; Vazyme, Nanjing, China). cDNA was quantified by Qubit 3.0 (Thermo Fisher) and 5 ng cDNA was used for DNA library construction with TruePrep DNA Library Prep Kit V2 for Illumina (TD502, Vazyme) following the manufacturer's instructions.

RNA-seq data processing

For RNA-seq analysis of all data, we downloaded the human reference genome (genome assembly: GRCh38) from the Ensembl database and used the HISAT2 software (version 2.2.1, <https://daehwankimlab.github.io/hisat2/>) for read alignment with a default setting after removing adaptor sequences and low-quality reads by fastp (version 0.12.4, <https://github.com/OpenGene/fastp>). The gene-level quantification approach was used to aggregate raw counts of mapped reads using the featureCounts tool. The expression level of each gene was quantified in terms of the normalized fragments per kilobase of transcript per million mapped reads (FPKM). Total genes of chromosome X and chromosome 1 were extracted, and the geometric mean FPKM of chromosomal expressed genes was calculated for each sample. Each FPKM value was incremental by one (FPKM + 1) for the calculation of geometric mean FPKM. Next, we used the R package DESeq2 (version 1.46.0, <https://bioconductor.org/packages/release/bioc/html/DESeq2.html>) for differential gene expression analysis. GO analysis (online, <https://www.geneontology.org/>) of screened DEGs was performed using the R package clusterProfiler. Functional annotation analysis of the screened differentially expressed genes using KOBAS (online, <http://bioinfo.org/kobas/annotate/>).

CUT&Tag library preparation

CUT&Tag libraries were prepared as previously described. Briefly, every 1×10^3 cells from a dish were pooled for one group. All groups were used for H4K16ac CUT&Tag DNA library construction with Hyperactive Universal CUT&Tag Assay Kit for Illumina (TD903, Vazyme) following the manufacturer's instructions. cDNA was quantified by Qubit 3.0.

CUT&Tag data analysis

The CUT&Tag paired-end reads were aligned to the human genome (hg38) using Bowtie 2 (version 2.2.5), which was downloaded from <https://sourceforge.net/projects/bowtie-bio/files/bowtie2/2.2.5/>. Prior to alignment, adaptor sequences and low-quality reads were removed using fastp (version 0.12.4, available at <https://github.com/OpenGene/fastp>). For the alignment of H3K27ac paired-end reads to the human reference genome GRCh38, Bowtie2 was employed with specific parameters: `-local -very-sensitive -no-unal -nomixed -no-discordant -phred33 -I 10 -X 700`.

Following alignment, PCR duplicates were removed using Picard software, which can be accessed at <https://github.com/broadinstitute/picard>. After assessing the correlation among biological replicates, the replicate reads from the two groups were merged using Samtools' 'merge' function. The resulting BAM files were then converted to BED format using BEDTools. Peak calling was performed on the merged files using MACS2 software, with peaks having a false discovery rate (FDR) $\leq 5\%$ being selected for downstream analysis.

Peak annotation was carried out using the R package ChIPseeker with default parameters. For peak comparison and overlap analysis, BEDTools was utilized. Quantitative analysis was based on the calculation of RPKM values from the merged BAM files, which was accomplished using the bamCoverage tool from the DeepTools software suite <https://test-argparse-readoc.readthedocs.io/en/latest/>. Finally, the H3K27ac CUT&Tag data were visualized using IGV, available at <https://igv.org/>.

Compass predictive analysis

Enter the matrix of routine transcriptome gene expression for calculation, convert reaction encoding into metabolic pathways based on the reaction penalties reflected in the results, and the Recon2 meta information, transform reaction penalties, and use Wilcoxon for differential analysis.

Statistics analysis

RNA-seq data were statistically analyzed using R software (version 4.2.3, <https://www.r-project.org/>). Differentially expressed genes were analyzed using the Wilcoxon rank-sum test, and p-values were adjusted using the Benjamini-Hochberg method. Data are presented as mean \pm standard error of the mean (SEM). RT-qPCR data were evaluated for differences between means using a two-tailed Student's t-test. A p-value of < 0.05 was considered statistically significant. Immunofluorescence intensity was statistically analyzed using ImageJ software (version 1.5, <https://imagej.net/ij/>) in combination with the two-tailed t-test of GraphPad Prism software (version 10.1.2, <https://www.graphpad.com/updates/prism-10-1-2-release-notes>). Experiments such as AP colony counting and cell viability were analyzed using Welch's one-tailed t-test.

Data availability

Publicly available datasets analyzed in this work are available in GEO. All sequencing data of hESCs generated in this study have been deposited in GEO under accession GSE268203.

Received: 15 November 2024; Accepted: 21 February 2025

Published online: 27 February 2025

References

- Wei, X. et al. Bach1 regulates self-renewal and impedes mesendodermal differentiation of human embryonic stem cells. *Sci. Adv.* **5**, eaau7887 (2019).
- Yamanaka, S. Pluripotent stem cell-based cell therapy—promise and challenges. *Cell. Stem Cell.* **27**, 523–531 (2020).
- Tian, Z., Yu, T., Liu, J., Wang, T. & Higuchi, A. Introduction to stem cells. *Prog. Mol. Biol. Transl. Sci.* **199**, 3–32 (2023).
- Au, K. F. & Sebastiano, V. The transcriptome of human pluripotent stem cells. *Curr. Opin. Genet. Dev.* **28**, 71–77 (2014).
- Hayashi, Y. et al. Structure-based discovery of NANOG variant with enhanced properties to promote self-renewal and reprogramming of pluripotent stem cells. *Proc. Natl. Acad. Sci. U.S.A.* **112**, 4666–4671 (2015).
- Okita, K., Nakagawa, M., Hyenjong, H., Ichisaka, T. & Yamanaka, S. Generation of mouse induced pluripotent stem cells without viral vectors. *Sci. (New York N Y)*. **322**, 949–953 (2008).
- Ma, T., Wang, Z., Guo, Y. & Pei, D. The C-terminal pentapeptide of Nanog Tryptophan repeat domain interacts with Nac1 and regulates stem cell proliferation but not pluripotency. *J. Biol. Chem.* **284**, 16071–16081 (2009).
- Carey, B. W., Finley, L. W., Cross, J. R., Allis, C. D. & Thompson, C. B. Intracellular α -ketoglutarate maintains the pluripotency of embryonic stem cells. *Nature* **518**, 413–416 (2015).
- Intlekofer, A. M. & Finley, L. W. S. Metabolic signatures of cancer cells and stem cells. *Nat. Metabolism* **1**, 177–188 (2019).
- Martello, G. & Smith, A. The nature of embryonic stem cells. *Annu. Rev. Cell Dev. Biol.* **30**, 647–675 (2014).
- Lee, H. Y. & Hong, I. S. Metabolic regulation and related molecular mechanisms in various stem cell functions. *Curr. Stem Cell Res. Therapy* **15**, 531–546 (2020).
- Zhu, Q. et al. O-GlcNAcylation regulates the methionine cycle to promote pluripotency of stem cells. *Proc. Natl. Acad. Sci. U.S.A.* **117**, 7755–7763 (2020).
- Munir, R., Lisee, J., Swinnen, J. V. & Zaidi, N. Lipid metabolism in cancer cells under metabolic stress. *Br. J. Cancer* **120**, 1090–1098 (2019).
- Yi, Y. et al. Fatty acid synthesis and oxidation regulate human endoderm differentiation by mediating SMAD3 nuclear localization via acetylation. *Dev. Cell.* **58**, 1670–1687e1674 (2023).

15. Lu, H., Tian, Z., Cui, Y., Liu, Z. & Ma, X. Chlorogenic acid: A comprehensive review of the dietary sources, processing effects, bioavailability, beneficial properties, mechanisms of action, and future directions. *Compr. Rev. Food Sci. Food Saf.* **19**, 3130–3158 (2020).
16. Naveed, M. et al. Chlorogenic acid (CGA): A Pharmacological review and call for further research. *Biomed. Pharmacother. Biomed. Pharmacother.* **97**, 67–74 (2018).
17. Wu, Y. et al. The effect of chlorogenic acid on *Bacillus subtilis* based on metabolomics. *Molecules* **25** (2020).
18. Pimpley, V., Patil, S., Srinivasan, K., Desai, N. & Murthy, P. S. The chemistry of chlorogenic acid from green coffee and its role in attenuation of obesity and diabetes. *Prep Biochem. Biotechnol.* **50**, 969–978 (2020).
19. Hayakawa, S. et al. Anti-Cancer effects of green tea Epigallocatechin-3-Gallate and coffee chlorogenic acid. *Molecules* **25** (2020).
20. Liang, N. & Kitts, D. D. Chlorogenic acid (CGA) isomers alleviate Interleukin 8 (IL-8) production in Caco-2 cells by decreasing phosphorylation of p38 and increasing cell integrity. *Int. J. Mol. Sci.* **19** (2018).
21. Santana-Galvez, J., Cisneros-Zevallos, L. & Jacobo-Velazquez, D. A. Chlorogenic acid: recent advances on its dual role as a food additive and a nutraceutical against metabolic syndrome. *Molecules* **22** (2017).
22. Tamura, H. et al. Anti-human immunodeficiency virus activity of 3,4,5-tricaffeoylquinic acid in cultured cells of lettuce leaves. *Mol. Nutr. Food Res.* **50**, 396–400 (2006).
23. Bruckbauer, A. & Zemel, M. B. Synergistic effects of polyphenols and methylxanthines with leucine on AMPK/Sirtuin-mediated metabolism in muscle cells and adipocytes. *PLoS One* **9**, e89166 (2014).
24. Ma, K. et al. Chlorogenic acid from Burdock roots ameliorates oleic acid-Induced steatosis in HepG2 cells through AMPK/ACC/CPT-1 pathway. *Molecules* **28** (2023).
25. Zhou, Y. et al. Chlorogenic acid from honeysuckle improves hepatic lipid dysregulation and modulates hepatic fatty acid composition in rats with chronic endotoxin infusion. *J. Clin. Biochem. Nutr.* **58**, 146–155 (2016).
26. Cornacchia, D. et al. Lipid deprivation induces a stable, Naive-to-Primed intermediate state of pluripotency in human PSCs. *Cell. Stem Cell.* **25**, 120–136e110 (2019).
27. Tajik, N., Tajik, M., Mack, I. & Enck, P. The potential effects of chlorogenic acid, the main phenolic components in coffee, on health: A comprehensive review of the literature. *Eur. J. Nutr.* **56**, 2215–2244 (2017).
28. Bhandarkar, N. S., Brown, L. & Panchal, S. K. Chlorogenic acid attenuates high-carbohydrate, high-fat diet-induced cardiovascular, liver, and metabolic changes in rats. *Nutr. Res. (New York N Y)* **62**, 78–88 (2019).
29. Xue, N., Liu, Y., Jin, J., Ji, M. & Chen, X. Chlorogenic acid prevents UVA-Induced skin Photoaging through regulating collagen metabolism and apoptosis in human dermal fibroblasts. *Int. J. Mol. Sci.* **23** (2022).
30. Kong, L. et al. Chlorogenic acid and caffeine combination attenuates adipogenesis by regulating fat metabolism and inhibiting adipocyte differentiation in 3T3-L1 cells. *J. Food Biochem.* **45**, e13795 (2021).
31. Meng, S., Cao, J., Feng, Q., Peng, J. & Hu, Y. Roles of chlorogenic Acid on regulating glucose and lipids metabolism: a review. *Evidence-based complementary and alternative medicine: eCAM* 801457 (2013). (2013).
32. Roy, D. G. et al. Methionine metabolism shapes T helper cell responses through regulation of epigenetic reprogramming. *Cell Metabol.* **31**, 250–266e259 (2020).
33. Yu, W. et al. One-Carbon metabolism supports S-Adenosylmethionine and histone methylation to drive inflammatory macrophages. *Mol. Cell* **75**, 1147–1160e1145 (2019).
34. Simon, M. D. et al. High-resolution Xist binding maps reveal two-step spreading during X-chromosome inactivation. *Nature* **504**, 465–469 (2013).
35. Mews, P. et al. Acetyl-CoA synthetase regulates histone acetylation and hippocampal memory. *Nature* **546**, 381–386 (2017).
36. He, W., Li, Q. & Li, X. Acetyl-CoA regulates lipid metabolism and histone acetylation modification in cancer. *Biochim. Et Biophys. Acta Reviews cancer.* **1878**, 188837 (2023).
37. Tabe, Y., Konopleva, M. & Andreeff, M. Fatty acid metabolism, bone marrow adipocytes, and AML. *Front. Oncol.* **10**, 155 (2020).
38. Guttenplan, K. A. et al. Neurotoxic reactive astrocytes induce cell death via saturated lipids. *Nature* **599**, 102–107 (2021).
39. Wang, T. et al. JAK/STAT3-regulated fatty acid β -oxidation is critical for breast cancer stem cell self-renewal and chemoresistance. *Cell Metabol.* **27**, 136–150e135 (2018).
40. Khoa, L. T. P. et al. Histone acetyltransferase MOF blocks acquisition of quiescence in ground-state ESCs through activating fatty acid oxidation. *Cell. Stem Cell.* **27**, 441–458e410 (2020).
41. Tsogetbaatar, E., Landin, C., Minter-Dykhouse, K. & Folmes, C. D. L. Energy metabolism regulates stem cell pluripotency. *Front. Cell. Dev. Biology.* **8**, 87 (2020).
42. Li, Y. J. et al. Fatty acid oxidation protects cancer cells from apoptosis by increasing mitochondrial membrane lipids. *Cell. Rep.* **39**, 110870 (2022).
43. Wang, Y. et al. The multiple facets of acetyl-CoA metabolism: Energetics, biosynthesis, regulation, acylation and inborn errors. *Mol. Genet. Metab.* **138**, 106966 (2023).
44. Hou, W. et al. Network characterization linc1393 in the maintenance of pluripotency provides the principles for LncRNA targets prediction. *iScience* **26**, 107469 (2023).

Author contributions

J.Z., Q.Z. and W.C. conceived and designed the study. M.Z., Q.W. and J.J. performed all cell experiment with contributions from W.C., L.Z., Y.C. L.C. and W.H analyzed the data with contributions from M.Z., L.Z., C.Z. and X.L. J.Z., W.C. and Q.K. supervised the project. J.Z., M.Z., and W.C. wrote the manuscript.

Funding

This work was supported by the Research Special Project of Zhejiang University of Traditional Chinese Medicine Affiliated Hospital (2024FSYYZY11).

Declarations

Competing interests

The authors declare no competing interests.

Additional information

Supplementary Information The online version contains supplementary material available at <https://doi.org/10.1038/s41598-025-91582-z>.

Correspondence and requests for materials should be addressed to J.Z., Q.Z. or W.C.

Reprints and permissions information is available at www.nature.com/reprints.

Publisher's note Springer Nature remains neutral with regard to jurisdictional claims in published maps and institutional affiliations.

Open Access This article is licensed under a Creative Commons Attribution-NonCommercial-NoDerivatives 4.0 International License, which permits any non-commercial use, sharing, distribution and reproduction in any medium or format, as long as you give appropriate credit to the original author(s) and the source, provide a link to the Creative Commons licence, and indicate if you modified the licensed material. You do not have permission under this licence to share adapted material derived from this article or parts of it. The images or other third party material in this article are included in the article's Creative Commons licence, unless indicated otherwise in a credit line to the material. If material is not included in the article's Creative Commons licence and your intended use is not permitted by statutory regulation or exceeds the permitted use, you will need to obtain permission directly from the copyright holder. To view a copy of this licence, visit <http://creativecommons.org/licenses/by-nc-nd/4.0/>.

© The Author(s) 2025